Brief Communications

Bulk Loading of Calcium Indicator Dyes to Study Astrocyte Physiology: Key Limitations and Improvements Using Morphological Maps

Alexander M. B. Reeves,[1] Eiji Shigetomi,[1] and Baljit S. Khakh[1,2]

Departments of [1]Physiology and [2]Neurobiology, David Geffen School of Medicine, University of California, Los Angeles, Los Angeles, California 90095

Calcium signaling has been studied in astrocyte cell bodies using bulk loading of calcium indicator dyes, and astrocytes are known to display intracellular calcium transients. An assumption in recent data on the neuronal impact of somatic astrocyte calcium transients has been that bulk loading reflects signaling in relevant astrocyte compartments such as processes. We assessed bulk loading using Sholl analysis (Sholl, 1953) of astrocytes loaded with common calcium indicator dyes and compared these data with Sholl analysis of astrocyte morphology. In the CA1 region of the hippocampus from rats, we found that bulk loading of calcium indicator dyes only reports on calcium signals within the soma and in the most proximal processes, leaving ~90% of the area of an astrocyte and its extensive processes unsampled. By using morphological reconstructions as "maps" after the imaging session, we present simple procedures that remedy these shortfalls and permit reliable detection of calcium transients in distal astrocyte processes. The data thus reveal limitations in the interpretation of astrocyte calcium imaging data gathered with bulk loading and provide refinements to minimize these shortcomings.

Introduction

Astrocytes form close spatial relationships with neurons and blood vessels through extensive processes (Halassa et al., 2007; Attwell et al., 2010). These processes define astrocyte territories, allow them to tile the brain, and serve supportive roles. Increasing evidence also suggests that astrocytes participate in the regulation of neuronal function and whole animal physiology (Halassa and Haydon, 2010).

Early studies showed that under appropriate conditions, astrocytes in brain slices could be loaded with organic calcium indicator dyes (Porter and McCarthy, 1995). In view of the specificity and ease of these procedures, the method has been extensively used in astrocyte research (Fiacco et al., 2009). Importantly, calcium transients measured using bulk loading are often used in a correlative manner with simultaneous measurements of neuronal function. On the basis of such experiments, evidence indicates that astrocyte calcium signals cause changes in neuronal function (Pasti et al., 1997, 2001; Araque et al., 1998; Parpura and Haydon, 2000; Parri et al., 2001; Angulo et al., 2004; Fellin et al., 2004; Perea and Araque, 2005, 2007; Serrano et al., 2006; Ding et al., 2007; Lee et al., 2007; Navarrete and Araque, 2008; Shigetomi et al., 2008; Gordon et al., 2009; Bardoni et al., 2010). However, other studies suggest this is not the case (Fiacco et al., 2007; Petravicz et al., 2008; Agulhon et al., 2010).

An assumption in past work is that bulk loading reports on astrocyte calcium signals in physiologically relevant compartments. This assumption is important in all studies of astrocytes, but particularly for experiments that produce largely negative data (Agulhon et al., 2010). In light of this, and in view of the importance of astrocyte calcium signals, we set out to evaluate and improve bulk loading.

Materials and Methods

Preparation of brain slices. Briefly, Sprague–Dawley rats (P14–P20) of either sex were killed following institutional procedures (Shigetomi et al., 2008). Coronal slices of hippocampus (300 μm) were cut (Vibratome) and submerged at room temperature in artificial cerebrospinal fluid (aCSF) comprising (mM) 126 NaCl, 2.5 KCl, 1.3 $MgCl_2$, 10 D-glucose, 2.4 $CaCl_2$, 1.24 NaH_2PO_4, and 26 $NaHCO_3$ saturated with 95% O_2 and 5% CO_2. Astrocytes were patched with 4–9 MΩ borosilicate glass electrodes filled with an intracellular solution comprising (mM) 123 CsCl, 1 $MgSO_4$, 10 HEPES, 1 ATP, 0.2 GTP, pH 7.35, and 100 μM Alexa Fluor-488 (Alexa-488). The patched astrocytes displayed linear current–voltage relations (between −100 and + 60 mV), with no evidence of prominent voltage-dependent currents. The cells were identified as astrocytes based on their shapes (Shigetomi et al., 2008) and electrophysiological properties (resting membrane potential = −95 ± 2 mV; membrane resistance = 105 ± 24 MΩ; n = 7) and voltage-clamped at −80 mV using a Multiclamp 900A amplifier (Molecular Devices).

GFAP staining. For GFAP staining, we fixed hippocampal slices in 4% paraformaldehyde for 3 h at 4°C. We then washed the slices with 0.1 M PBS and incubated them in 0.5% Triton X-100 for 30 min at 4°C. Subsequently, we incubated the slices in 10% normal goat serum for 2 h at 4°C, followed by incubation with GFAP primary antibodies [66 μg/ml (1:500) from Abcam] for 24 h at 4°C. The slices were then washed in PBS and incubated in the secondary goat anti-chicken antibody (1:500) for 3 h at room temperature.

Received Jan. 8, 2011; revised May 10, 2011; accepted May 13, 2011.

Author contributions: A.M.B.R., E.S., and B.S.K. designed research; A.M.B.R. and E.S. performed research; A.M.B.R. and E.S. analyzed data; A.M.B.R., E.S., and B.S.K. wrote the paper.

This work was supported by the Whitehall Foundation, the National Institutes of Health (Grants NS071292, NS063186-02S1, and NS060677), and a Stein/Oppenheimer Endowment Award (B.S.K.). Thanks to Tiffany M. Schmidt for tips on Sholl analysis. Thanks also to the Astrocyte Biology and Biophysics Affinity Group at the University of California, Los Angeles, for discussions, and Michael Sofroniew for comments.

Correspondence should be addressed to Dr. Baljit S. Khakh, Department of Physiology, University of California, Los Angeles, 10833 Le Conte Avenue, Los Angeles, CA 90095-1751. E-mail: bkhakh@mednet.ucla.edu.

DOI:10.1523/JNEUROSCI.0127-11.2011

 0270-6474/11/319353-06$15.00/0

Confocal imaging of Ca^{2+} dynamics and dialysis of astrocytes with Alexa-488. Brain slices were loaded at room temperature in the dark with 5 μM Fluo-4AM [or 5 μM Oregon Green BAPTA-1 AM (OGB-AM) and SR101; Invitrogen] in aCSF for 60 min, then transferred to dye-free aCSF for at least 30 min. Cells and slices were imaged using an Olympus Fluoview 300 laser scanning confocal microscope. For Alexa-488 dialysis, the astrocytes were held at −80 mV and depolarized to 60 mV for 100 ms every 30 s to monitor access resistance. During this procedure, coupled astrocytes were also dialyzed with Alexa-488; however, we only analyzed the Alexa-488 signals from the patched cell.

Morphological reconstructions and Sholl analysis. For astrocytes bulk loaded with Fluo-4AM or OGB-AM, we used the 488 nm line of an argon laser and a 510 nm high-pass emission filter. When imaging SR101 and Fluo-4 simultaneously, we used a 570 nm dichroic mirror and appropriate emission filters. The other fluorophores (GFAP staining and Alexa-488) were imaged using similar settings. For the Fluo-4AM-loaded and OGB-AM-loaded astrocytes (after detecting calcium transients), we selected astrocytes from the stratum radiatum region and collected image stacks in 1 μm planes. The cells were 20–90 μm from the slice surface and the image stacks covered ~15 μm in *z*-axis depth. Images were gathered with a 40× water-immersion lens with a numerical aperture of 0.8 (Olympus). Image stacks of fluorescent astrocytes were traced and reconstructed as 2D binarized representations using ImageJ (National Institutes of Health). We used the Sholl method of concentric circles (Sholl, 1953) using an ImageJ regime. Each cell was thus analyzed by selecting the center of its soma and then running the Sholl analysis procedure, which counts the number of intersections at circles of increasing radii from the center. The image stacks of astrocytes also allowed us to make 2D reconstructions of their morphology by tracing regions of interest (ROIs) around the soma and processes. For the tracing, thresholds were chosen on a cell-by-cell basis so as to include as many fine processes as possible (threshold for the distal processes was twofold higher than background). Beginning with the soma, pixels were included in a given astrocyte only if they were continuous with the rest of the astrocyte. It is likely that this procedure underestimated astrocyte complexity because light microscopy cannot reveal the finest astrocyte processes (Ventura and Harris, 1999). For the experiments in Figure 3, we performed Fluo-4 calcium imaging experiments in a single optical plane and performed morphological reconstructions from a *z* series of images. We then used the reconstructions as a *post hoc* map to determine whether more calcium transients could be detected from the Fluo-4 time series images. Transients, detected with the benefit of the reconstructions, could be easily assigned to a particular cell because they fell on its reconstructed morphological map.

Statistical analysis and generation of graphs. Data were analyzed using pCLAMP9 (Molecular Devices) and Origin 8 (OriginLab Corp). Imaging data were analyzed using ImageJ. Statistical tests were run in GraphPad InStat 3.06 (GraphPad Software Inc.). Data are shown as mean ± SEM from *n* determinations.

Chemicals. All reagents were from VWR Scientific, Invitrogen, Sigma-Aldrich, Tocris-Cookson, or Ascent Scientific.

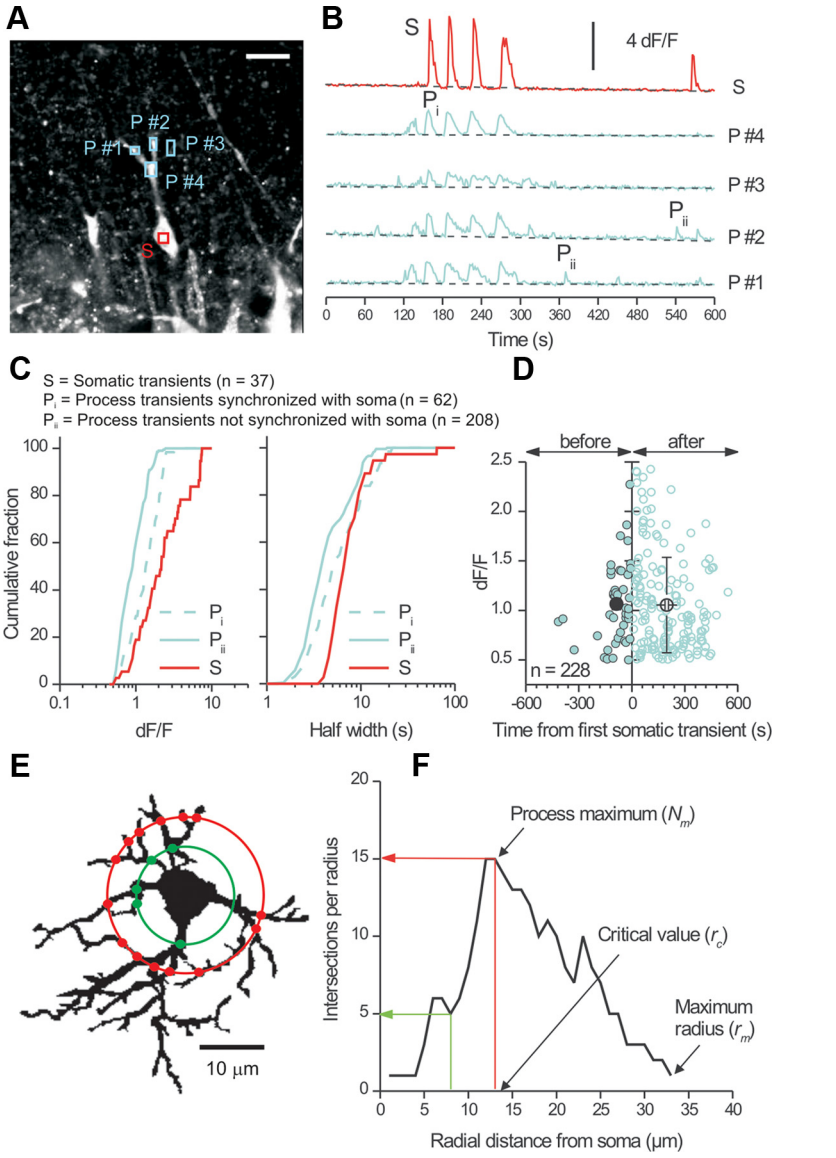

Figure 1. Differences between calcium signals in astrocyte somata and processes. ***A***, Confocal image of an astrocyte from the stratum radiatum region of a hippocampal slice (P16) loaded with Fluo-4AM. The soma and two processes were visible in this optical plane and regions of interest were selected in the soma (S) and processes (P #1–P #4). Scale bar, 15 μm. ***B***, dF/F traces for the regions shown in ***A*** plotted over time. ***C***, Left graph, peak dF/F values for calcium signals measured in the somata and processes of astrocytes. The three distributions were significantly different (Kolmogorov–Smirnov test; bin size = 0.025 dF/F). Right graph, distribution of calcium transient half-widths. Kolmogorov–Smirnov analysis showed that the S and P_i as well as S and P_{ii} transients differed significantly in duration, whereas the P_i and P_{ii} transients did not. ***D***, Scatter plot of peak dF/F values for P_{ii} type transients plotted against their occurrence time relative to the first somatic signal in the cells. ***E***, Flattened 2D image from a 3D reconstruction of a GFAP-labeled astrocyte used to schematically illustrate Sholl analysis. Circles of increasing diameter from the center of the soma were drawn in 1 μm intervals and the number of intersections with the cell measured (red and green dots). ***F***, Exemplar Sholl plot for the astrocyte shown in ***E***.

Results

Initial observations

We use the words "loaded astrocytes" to indicate cells that had been bulk loaded with Fluo-4AM or OGB-AM. We use the word "dialyzed" to indicate cells that had been filled via the patch pipette.

We incubated hippocampal slices with Fluo-4AM, resulting in loaded astrocytes in the stratum radiatum, which displayed spontaneous calcium transients (Nett et al., 2002). The peak amplitude (1.05 ± 0.04 dF/F) and time course ($t_{(0.5)}$ = 12.7 ± 1.5 s) of these calcium signals were similar to previous studies (188 transients from n = 58 cells).

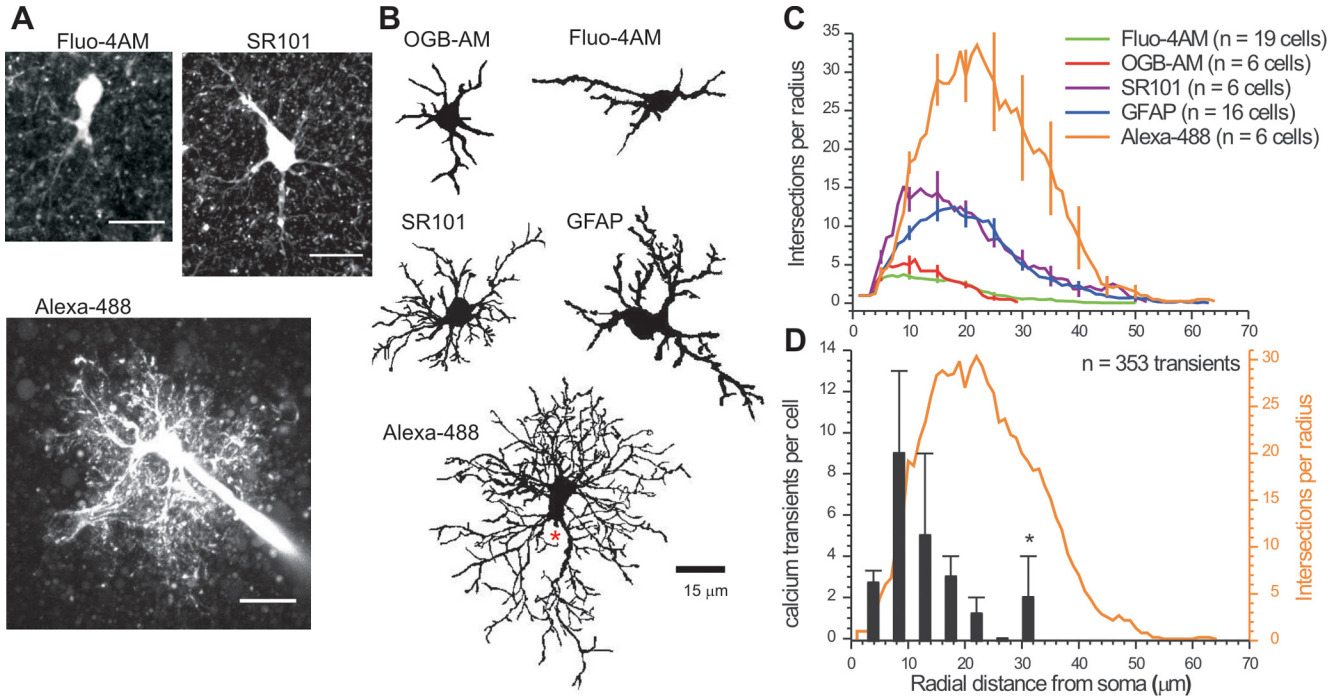

Figure 2. Morphological Sholl analysis of astrocytes. ***A***, Representative maximum projection images from confocal *z* series for astrocytes loaded with Fluo-4AM, labeled with SR101, or dialyzed with Alexa-488. Scale bars, 15 μm. ***B***, 2D representations of astrocytes loaded with calcium indicator dyes (OGB-AM, Fluo-4AM) and those labeled with SR101 and GFAP, as well as an astrocyte dialyzed with Alexa-488. In the Alexa-488 image, the approximate position of the patch pipette is shown with a red asterisk. ***C***, Average Sholl plots from reconstructions such as those shown in ***B***. ***D***, Average Alexa-488 Sholl plot (orange line and axis) superimposed on the number of calcium transients measured at increasing distances from the soma (black bars) for Fluo-4-loaded astrocytes (Fig. 1; $n = 15$ astrocytes and 353 transients).

Next, we identified single astrocytes and examined spontaneous signals in their somata and processes in a single confocal plane (Fig. 1*A*). We imaged astrocytes for 10 min and identified ROIs in the somata and processes (Fig. 1*B*). We identified three classes of calcium signals: (1) somatic transients, (2) transients in processes that were synchronized with those in the soma (Fig. 1*B*), and (3) transients in processes that were not synchronized with those in the soma (Fig. 1*B*). We named these classes S, P_i, and P_{ii}, respectively, in Figure 1, *B* and *C*, and designated them "synchronized" if they occurred during the half-width of a somatic transient (~7 s) (Fig. 1*C*). These analyses showed that the largest transients were in the soma, followed by synchronized events in the processes (P_i) (Fig. 1*C*). Thus, the smallest signals were transients in the processes (P_{ii}) that were not synchronized with those in the soma ($p < 0.05$ Kolmogorov–Smirnov test) (Fig. 1*C*). In the example of Figure 1*B*, somatic transients were always accompanied by P_i type transients in the processes.

We also analyzed the time difference between the peak of P_{ii} type calcium signals in relation to somatic signals (Fig. 1*C*) and made three observations. First, P_{ii} type transients occurring before and after somatic signals displayed similar amplitudes (Fig. 1*D*). Second, the P_{ii} type transients before somatic ones occurred within a narrower time window than those that followed (-87 ± 13 s vs 197 ± 10 s) (Fig. 1*D*). In relation to this, the first somatic calcium transient occurred at 200 ± 60 s during 600 s imaging experiments, that is, not significantly different from it occurring randomly at 300 s ($p = 0.1395$; $n = 8$). Third, the P_{ii} type transients that follow somatic transients were more numerous by 3.8-fold than those that preceded somatic signals (180 vs 47 transients) (Fig. 1*D*), even when one accounts for the fact the first somatic calcium signal occurred at ~200 s (implying a twofold difference). It will be interesting to explore these relationships further, but from the perspective of this undertaking, the data (Fig. 1*A–C*) recall previous studies (Nett et al., 2002) and serve as a basis to evaluate bulk loading.

Table 1. Sholl analysis of astrocytes

	Calcium indicators		Morphology markers		
	Fluo-4AM	OGB-AM	GFAP	SR101	Alexa-488
Process maximum (N_m)[a]	6 ± 0.3	7 ± 1	15 ± 2	18 ± 2	36 ± 3
Critical value (r_c: μm)	13 ± 1	9 ± 1	19 ± 1	15 ± 2	19 ± 1
Maximum radius (μm)	30 ± 2	25 ± 1	45 ± 2	43 ± 3	50 ± 3
Number of primary branches (N_p)[a]	4.0 ± 0.4	4.2 ± 0.5	5.9 ± 0.6	8.3 ± 0.6	6.3 ± 0.6[b]
Integrated Sholl plot (intersection · μm)	73 ± 7	78 ± 2	288 ± 26	341 ± 25	749 ± 94
Schoenen ramification index (N_m/N_p)[a]	1.5 ± 0.1	1.6 ± 0.2	2.9 ± 0.3	2.3 ± 0.3	5.4 ± 0.6
n	19	6	16	6	6

[a]Tukey's ANOVA test ($p < 0.05$) shows that Fluo-4 loaded cells displayed significantly fewer processes as compared with GFAP, SR101, and Alexa-488 astrocytes, but that there were no significant differences between GFAP and SR101 cells. The greatest number of processes and morphological complexity was seen for the astrocytes loaded with Alexa-488.

[b]The number of primary processes is lower for the Alexa-488 cells as compared with the SR101 cells because the patch pipette obscures some primary processes (Fig 2*A*).

Sholl morphological analysis of astrocytes loaded with calcium indicator dyes

Using Sholl morphological analysis (Sholl, 1953), we determined how well bulk loading sampled astrocytes. Figure 1*E* illustrates the Sholl method for an astrocyte labeled for GFAP. Sholl analysis was performed by overlaying circles of increasing diameter (in 1 μm steps) out from the center of the soma of an astrocyte and by counting the number of intersections the astrocyte makes with each (Fig. 1*F*). We then plotted the number of intersections per

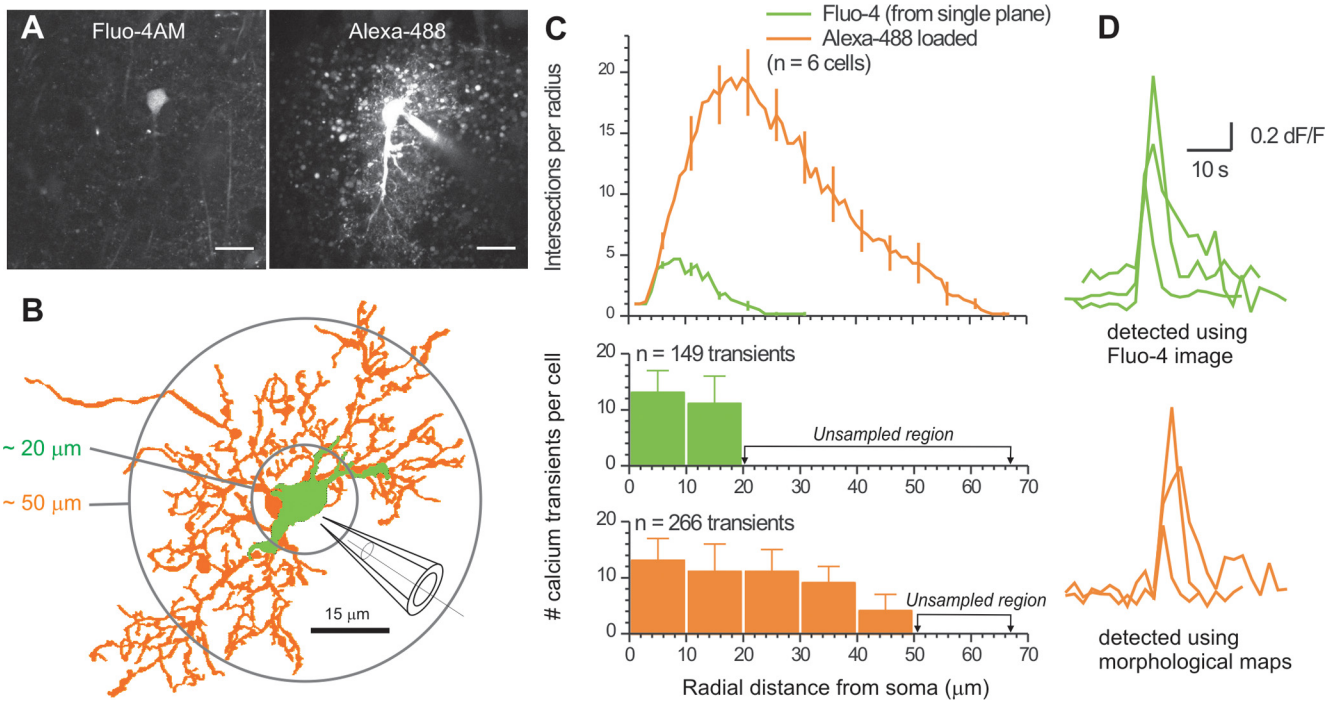

Figure 3. Morphological maps improve detection of calcium transients in astrocyte processes. ***A***, Left, Representative image of an astrocyte loaded with Fluo-4AM (acquired in a single confocal plane). Right, Representative image of the same astrocyte dialyzed with Alexa-488 after the calcium imaging session. Scale bars, 15 μm. ***B***, 2D representation of another astrocyte loaded with Fluo-4 (from one confocal plane; green). A 2D representation of the same astrocyte is shown for the *z* series after loading with Alexa-488 via the patch pipette (orange). ***C***, Top, Average Sholl plots from reconstructions such as those shown in ***B***. Bottom, Number of calcium transients measured at increasing distances from the soma in 10 μm bins. The green bars correspond to transients measured in one confocal plane from the Fluo-4 image. The orange bars represent transients detected using 2D morphological maps of the Alexa-488 *z* series: the sampled region was larger, as shown by the circles in ***B***. ***D***, Exemplar calcium transient traces for the two different conditions of analysis indicated.

circle against radial distance from the soma (Fig. 1*F*). From such Sholl plots, the process maximum (N_m) represents the highest number of intersections an astrocyte makes (Fig. 1*F*), the critical value (r_c) was the distance from the soma at which N_m occurs, and the maximum radius was the maximum width of the Sholl plot. We also measured the number of primary branches emanating directly from the soma of each astrocyte (N_p) and calculated the Schoenen ramification index (as N_m/N_p), which quantifies overall branching (Schoenen, 1982).

We performed Sholl analysis on astrocytes bulk loaded with commonly used calcium indicator dyes (Fluo-4AM and OGB-AM) and compared these with Sholl plots from GFAP antibody-stained and SR101-labeled astrocytes (Kafitz et al., 2008). To quantify astrocytes in their entirety, we dialyzed astrocytes with Alexa-488 via a patch-clamp pipette (Shigetomi et al., 2008). Representative fluorescence images and reconstructions are shown in Figure 2, *A* and *B*. In relation to the images and Sholl plots for Fluo-4 and OGB, those for Alexa-488 were much more complex, with numerous branches and fine processes. Light microscopy is insufficient to image the finest astrocyte processes (Ventura and Harris, 1999), but the maximal extent of astrocytes determined by Sholl analysis recalls past estimates (Halassa et al., 2007) and was not limited by the method because Sholl plots for interneurons extended to a maximum radius of 170 ± 10 μm ($n = 4$).

The average data presented in Figure 2*C* and parameters shown in Table 1 show that bulk loading (1) is only adequate to image the somata of astrocytes, (2) underestimates the number of primary branches, (3) fails to capture any processes beyond ~25 μm, and (4) overall reports on only ~10% of the complexity of an astrocyte (Table 1). Next, we plotted the location of spontaneous calcium transients ($n = 353$ from 15 cells) (Fig. 1) along astrocyte processes in relation to the average Sholl plot for Alexa-488-loaded cells (Fig. 2*D*). This analysis shows that most calcium signals were measured in the first ~20 μm for 14/15 astrocytes (1/15 cells showed transients ~30 μm from the soma; Fig. 2*D*, asterisk). Thus, almost no calcium signals could be measured when the astrocytes reached their greatest complexity and none were measured in distal and terminal processes (Fig. 2*D*).

Improved detection of calcium transients in astrocyte processes using morphological "maps"

We attempted to capitalize on experiences with Sholl analysis to improve detection of calcium transients in astrocyte processes. We imaged Fluo-4-loaded astrocytes in a single confocal plane (for 10 min) to monitor calcium transients. We then patched the cells and acquired *z*-series images following loading with Alexa-488 via the patch pipette ($n = 6$) (Fig. 3*A*). *Post hoc*, we performed morphological reconstructions and Sholl analysis for astrocytes under these two conditions (color coded in Fig. 3*B*,*C*). For the Fluo-4-loaded cells, we detected calcium transients only within the first ~20 μm from the soma (Fig. 3*B*,*C*). However, when we used the reconstructions for the Alexa-488 *z* series as a morphological map to look for calcium transients, we detected significantly more transients per cell up to 50 μm from the soma (Fig. 3*B*,*C*). These data indicate that using astrocyte morphological maps improves calcium transient detection by ~81% (from 149 transients to 266). Greater numbers of calcium transients were measured because they were easier to identify and assign to processes rather than the neuropil. Examples of calcium transients measured in this way are shown in Figure 3*D*. The transients in

processes identified with the aid of morphological maps displayed smaller peak dF/F values as compared with those measured using conventional methods near the soma (0.69 ± 0.02 vs 1.04 ± 0.06; $n = 272$ and 149; $p < 0.01$), whereas the kinetics were similar (6.3 ± 0.6 s vs 5.3 ± 0.2 s; $n = 272$ and 149; $p > 0.05$). The terminal $\sim$15 μm of the Sholl plot (Fig. 3*B*) from which we failed to detect calcium transients is likely because Fluo-4 was insufficiently loaded into these regions.

Discussion

The bulk loading method has been extensively used to study astrocytes. The assumption that bulk loading reports on astrocyte calcium in physiologically relevant compartments is important for experiments reporting that somatic astrocyte calcium transients do not affect neurons (Fiacco et al., 2007; Agulhon et al., 2010). In the absence of this assumption, the lack of a correlative relation between astrocyte somatic calcium and alterations in neuronal function may suggest that calcium was measured in an inappropriate astrocyte compartment. The issue is relevant because the ability of bulk loading to fully sample astrocytes has not been assessed. Moreover, unlike neurons, astrocytes do not display propagated electrical signals; therefore, there is no reason to surmise that somatic signals bear any predictable relation to those in astrocyte processes.

Our data show that existing bulk loading procedures do not sample the vast majority ($\sim$90%) of the processes of an astrocyte, but they do sample the soma. Our data also show that P_{ii} type spontaneous calcium signals in processes differ from those in the soma (Fig. 1). We interpret this to suggest that somatic signals cannot be used as a "surrogate measure" of those in processes, but it is important to note that we studied only spontaneous signals and not those evoked by exogenous neurotransmitters, which may spread along the cell. These issues are relevant given that astrocytes have been shown to signal via their processes (Gordon et al., 2009) and the fact that similar somatic calcium signals are known not to signal in an equivalent manner to neurons (Shigetomi et al., 2008). Moreover, patch-clamp-mediated dialysis of calcium indicator dyes does not remedy these shortfalls for hippocampal astrocytes (Agulhon et al., 2010) because this procedure is invasive and leads to rundown and loss of calcium signals within minutes (Nett et al., 2002). Our data showing that astrocytes are not fully sampled using bulk loading raise the issue of why. One simple explanation is that the volumes of fine processes are too meager to adequately fill with bulk loading methods and/or that there are significant diffusive barriers in the lumen of processes.

We demonstrated that reconstructions and morphological maps aid in the detection of calcium signals in processes. We suggest this procedure ought to be implemented in future studies that seek to study astrocyte calcium signals and how they affect neurons. In addition, transgenic mice expressing red fluorescent proteins in astrocytes could be used for morphological purposes in combination with appropriate calcium indicator dyes. Equally important, Sholl analysis provides precise data on what proportion of an astrocyte has been sampled. Perhaps this ought to be routinely performed on astrocytes so that the extent of loading can be compared between studies.

Further improvements are needed to measure calcium in terminal processes, for example, using improved genetically encoded calcium indicators (Atkin et al., 2009; Shigetomi et al., 2010). However, even these approaches are unlikely to yield data on very fine astrocyte processes (Ventura and Harris, 1999). In the interim, the implementation of the procedures described here will allow the quality of data gathered with bulk loading to be compared between studies and allow for improved detection of calcium signals in distal processes.

References

Agulhon C, Fiacco TA, McCarthy KD (2010) Hippocampal short- and long-term plasticity are not modulated by astrocyte Ca^{2+} signaling. Science 327:1250–1254.

Angulo MC, Kozlov AS, Charpak S, Audinat E (2004) Glutamate released from glial cells synchronizes neuronal activity in the hippocampus. J Neurosci 24:6920–6927.

Araque A, Sanzgiri RP, Parpura V, Haydon PG (1998) Calcium elevation in astrocytes causes an NMDA receptor-dependent increase in the frequency of miniature synaptic currents in cultured hippocampal neurons. J Neurosci 18:6822–6829.

Atkin SD, Patel S, Kocharyan A, Holtzclaw LA, Weerth SH, Schram V, Pickel J, Russell JT (2009) Transgenic mice expressing a cameleon fluorescent Ca^{2+} indicator in astrocytes and Schwann cells allow study of glial cell Ca^{2+} signals *in situ* and *in vivo*. J Neurosci Methods 181:212–226.

Attwell D, Buchan AM, Charpak S, Lauritzen M, Macvicar BA, Newman EA (2010) Glial and neuronal control of brain blood flow. Nature 468:232–243.

Bardoni R, Ghirri A, Zonta M, Betelli C, Vitale G, Ruggieri V, Sandrini M, Carmignoto G (2010) Glutamate-mediated astrocyte-to-neuron signalling in the rat dorsal horn. J Physiol 588:831–846.

Ding S, Fellin T, Zhu Y, Lee SY, Auberson YP, Meaney DF, Coulter DA, Carmignoto G, Haydon PG (2007) Enhanced astrocytic Ca^{2+} signals contribute to neuronal excitotoxicity after status epilepticus. J Neurosci 27:10674–10684.

Fellin T, Pascual O, Gobbo S, Pozzan T, Haydon PG, Carmignoto G (2004) Neuronal synchrony mediated by astrocytic glutamate through activation of extrasynaptic NMDA receptors. Neuron 43:729–743.

Fiacco TA, Agulhon C, Taves SR, Petravicz J, Casper KB, Dong X, Chen J, McCarthy KD (2007) Selective stimulation of astrocyte calcium *in situ* does not affect neuronal excitatory synaptic activity. Neuron 54:611–626.

Fiacco TA, Agulhon C, McCarthy KD (2009) Sorting out astrocyte physiology from pharmacology. Annu Rev Pharmacol Toxicol 49:151–174.

Gordon GR, Iremonger KJ, Kantevari S, Ellis-Davies GC, MacVicar BA, Bains JS (2009) Astrocyte-mediated distributed plasticity at hypothalamic glutamate synapses. Neuron 64:391–403.

Halassa MM, Haydon PG (2010) Integrated brain circuits: astrocytic networks modulate neuronal activity and behavior. Annu Rev Physiol 72:335–355.

Halassa MM, Fellin T, Takano H, Dong JH, Haydon PG (2007) Synaptic islands defined by the territory of a single astrocyte. J Neurosci 27:6473–6477.

Kafitz KW, Meier SD, Stephan J, Rose CR (2008) Developmental profile and properties of sulforhodamine 101-labeled glial cells in acute brain slices of rat hippocampus. J Neurosci Methods 169:84–92.

Lee CJ, Mannaioni G, Yuan H, Woo DH, Gingrich MB, Traynelis SF (2007) Astrocytic control of synaptic NMDA receptors. J Physiol 581:1057–1081.

Navarrete M, Araque A (2008) Endocannabinoids mediate neuron–astrocyte communication. Neuron 57:883–893.

Nett WJ, Oloff SH, McCarthy KD (2002) Hippocampal astrocytes *in situ* exhibit calcium oscillations that occur independent of neuronal activity. J Neurophysiol 87:528–537.

Parpura V, Haydon PG (2000) Physiological astrocytic calcium levels stimulate glutamate release to modulate adjacent neurons. Proc Natl Acad Sci U S A 97:8629–8634.

Parri HR, Gould TM, Crunelli V (2001) Spontaneous astrocytic Ca^{2+} oscillations *in situ* drive NMDAR-mediated neuronal excitation. Nat Neurosci 4:803–812.

Pasti L, Volterra A, Pozzan T, Carmignoto G (1997) Intracellular calcium oscillations in astrocytes: a highly plastic, bidirectional form of communication between neurons and astrocytes *in situ*. J Neurosci 17:7817–7830.

Pasti L, Zonta M, Pozzan T, Vicini S, Carmignoto G (2001) Cytosolic calcium oscillations in astrocytes may regulate exocytotic release of glutamate. J Neurosci 21:477–484.

Perea G, Araque A (2005) Properties of synaptically evoked astrocyte cal-

cium signal reveal synaptic information processing by astrocytes. J Neurosci 25:2192–2203.

Perea G, Araque A (2007) Astrocytes potentiate transmitter release at single hippocampal synapses. Science 317:1083–1086.

Petravicz J, Fiacco TA, McCarthy KD (2008) Loss of IP3 receptor-dependent Ca^{2+} increases in hippocampal astrocytes does not affect baseline CA1 pyramidal neuron synaptic activity. J Neurosci 28:4967–4973.

Porter JT, McCarthy KD (1995) GFAP-positive hippocampal astrocytes *in situ* respond to glutamatergic neuroligands with increases in $[Ca^{2+}]_i$. Glia 13:101–112.

Schoenen J (1982) The dendritic organization of the human spinal cord: the dorsal horn. Neuroscience 7:2057–2087.

Serrano A, Haddjeri N, Lacaille JC, Robitaille R (2006) GABAergic network activation of glial cells underlies hippocampal heterosynaptic depression. J Neurosci 26:5370–5382.

Shigetomi E, Bowser DN, Sofroniew MV, Khakh BS (2008) Two forms of astrocyte calcium excitability have distinct effects on NMDA receptor-mediated slow inward currents in pyramidal neurons. J Neurosci 28:6659–6663.

Shigetomi E, Kracun S, Sofroniew MV, Khakh BS (2010) A genetically targeted optical sensor to monitor calcium signals in astrocyte processes. Nat Neurosci 13:759–766.

Sholl DA (1953) Dendritic organization in the neurons of the visual and motor cortices of the cat. J Anat 87:387–406.

Ventura R, Harris KM (1999) Three-dimensional relationships between hippocampal synapses and astrocytes. J Neurosci 19:6897–6906.